Ecological Informatics 64 (2021) 101351

Contents lists available at ScienceDirect

Ecological Informatics

journal homepage: www.elsevier.com/locate/ecolinf

Implementation of a proactive system to monitor *Aedes aegypti* populations using open access historical and forecasted meteorological data

Exequiel Aguirre[a,b,*,1], Verónica Andreo[c,d,1], Ximena Porcasi[b,1], Laura Lopez[e], Claudio Guzman[e], Patricia González[e], Carlos M. Scavuzzo[b,c]

[a] *Universidad Nacional de Córdoba, Facultad de Matemática, Astronomía, Física y Computación, Grupo de Análisis Numérico y Computación, Av. Medina Allende s/n, X5000HUA Córdoba, Argentina*
[b] *Comisión Nacional de Actividades Espaciales, Falda del Cañete, Córdoba, Argentina*
[c] *Instituto de Altos Estudios Espaciales "Mario Gulich", Falda del Cañete, Córdoba, Argentina*
[d] *CONICET, Consejo Nacional de Investigaciones Científicas y Técnicas. Buenos Aires, Argentina*
[e] *Área de Epidemiología, Programa de Zoonosis, Manejo Integrado de Vectores (MIP), Córdoba, Argentina*

ARTICLE INFO

Keywords:
Decision support system
Precipitation
Population dynamics
Mathematical modeling
Forecast

ABSTRACT

Due to the global increase in mosquito-borne diseases outbreaks it is recommended to increase surveillance and monitoring of vector species to respond swiftly and with early warning indicators. Usually, however, the information about vector presence and activity seems to be insufficient to implement timely and effective control strategies. Here we present an improved mathematical model of *Aedes aegypti* population dynamics with the aim of making the Dengue surveillance system more proactive. The model considers the four life stages of the mosquito: egg, larva, pupa and adult. As driving factors, it incorporates temperature which affects development and mortality rates at certain stages, and precipitation which is known to affect egg submergence and hatching, as well as larval mortality associated with desiccation. Our mechanistic model is implemented as a free and stand-alone system that automatically retrieves all needed inputs, runs a simulation and shows the results. A major improvement in our implementation is the capacity of the system to predict the population dynamics of *Ae. aegypti* in the near future, given that it uses gridded weather forecast data. Hence, it is independent by meteorological station proximity. The model predictions are compared with field data from Córdoba City, Argentina. Although field data have high variability, an overall accordance has been observed. The comparison of results obtained using observed weather data, with the simulations based on forecasts, suggests that the modeled dynamics are accurate up to 15 days in advance. Preliminary results of *Ae. aegypti* population dynamics for a consecutive three-year period, spanning different eco-regions of Argentina, are presented, and demonstrate the flexibility of the system.

1. Introduction

Dengue is a rapidly spreading mosquito-borne disease with recent outbreaks throughout the Americas (PAHO/WHO, 2020). The main vector of dengue virus is *Aedes aegypti* (Linnaeus, 1762), a mosquito species originally from Africa (Souza-Neto et al., 2019) that, propagates under global warming, urbanization and globalization, has invaded many temperate areas of the world (Liu-Helmersson et al., 2019; Vezzani and Carbajo, 2008), reaching latitudes as far south as 40° S (Rubio et al., 2020a). This mosquito species is fully adapted to urban areas where it can fulfill all of its ecological needs (Powell and Tabachnick, 2013).

The dynamics of mosquito-borne diseases are assumed to be strongly linked to the abundance of the host vector. In this sense, the main recommendation from the World Health Organization (WHO) and the Pan American Health Organization (PAHO) is to conduct rigorous vector surveillance and control programs which make up an essential component of disease prevention (PAHO/WHO, 2020; WHO, 2020).

Unfortunately, as WHO explained, a weakness of Dengue prevention strategies is that in several cases they are reactive rather than proactive

* Corresponding author at: Universidad Nacional de Córdoba, Facultad de Matemática, Astronomía, Física y Computación, Grupo de Análisis Numérico y Computación, Av. Medina Allende s/n, X5000HUA Córdoba, Argentina.
E-mail address: exequiel.aguirre@mi.unc.edu.ar (E. Aguirre).
[1] These authors contributed equally to the work.

https://doi.org/10.1016/j.ecoinf.2021.101351
Received 26 October 2020; Received in revised form 29 May 2021; Accepted 4 June 2021
Available online 10 June 2021
1574-9541/

(WHO, 2010); implying that recording only lagged information about the presence or abundance of *Ae. aegypti* might be insufficient for a Dengue prevention system.

The populations of *Ae. aegypti* are regulated by exogenous (environmental) and endogenous (density-dependent) drivers (Yang et al., 2008). The combination of these drivers contribute to the characteristic oscillatory pattern of peaks and troughs in mosquito abundance over the course of a single year (Hone and Clutton-Brock, 2007). Temperature effects on mosquito biology are well documented, indeed, temperature accounts for most of the observed variation in larval development rates (Yang et al., 2008). Less studied, precipitation patterns could limit juvenile mosquito survival by overflowing larval breeding sites, or by drying them out (Costa et al., 2010). Indeed, immature stages of *Ae. aegypti* are predominantly linked to ephemeral habitats, i.e., breeding sites are limited in water volume and typically last for short periods of time. Such habitats include different types of disposable containers, tyres, tree holes, and small pools (Chandrasegaran et al., 2020; Vezzani et al., 2005). Importantly, *Ae. aegypti* females lay eggs on the walls of such containers just above water level in contrast with other species that directly lay eggs in the water (Christophers, 1960). For these reasons, temperature, precipitation and water amount in a container are considered in our model.

There are a number of approaches that have been developed to explain the basic causes underlying fluctuations in natural and controlled populations. To implement control measures, most studies have focused on describing and quantifying habitat associations and spatio-temporal distribution of vector species (Yang et al., 2009). As a way to reduce the gap between surveillance and prevention, different mechanistic models have been developed to better understand this biological system, explain temporal patterns, and forecast *Ae. aegypti*'s population dynamics. Initially, Focks et al. Focks et al. (1993) developed a deterministic model incorporating several biological processes (survival, development and fecundity) for four different life stages: egg, larvae, pupae and adult. Later on, Otero et al. Otero et al. (2006) introduced a minimalist temperature-driven deterministic differential equation model and an associated stochastic model (Kurtz, 1970; Kurtz, 1971; Otero et al., 2006), for these four life stages in regions with no dry season, thus not considering the dependence on rainfall for the hatching rate. More recently, Aznar et al. Aznar et al. (2013) developed an improved stochastic model which considers rainfall as the trigger for egg hatching. In this model, when rainfall surpasses a certain threshold, eggs will be considered wet and begin to hatch at a temperature-dependent rate. Here, we improved the deterministic model proposed by Otero et al. Otero et al. (2006) by including the effect of rainfall. We follow, however, a different approach than the one proposed by Aznar et al. Aznar et al. (2013). For a certain container (i.e., artificial recipient containing water that might be used by females to lay eggs), the water level (rainfall dependent) and the position where eggs are laid is modeled explicitly. Hence, a container with water level larger than zero cm is considered a breeding site; and only submerged eggs will hatch at a rate that depends on temperature.

One of the biggest challenges in previous climate-driven models, was to obtain meteorological information for places where no weather station is available. For this reason, our meteorological data sources consist of grids from atmospheric reanalysis, satellite technology and weather forecast models. The latter aims to make the population dynamics model a more proactive tool, allowing users to forecast abundance values in advance, according to predicted weather conditions.

In the present work we aim to: i) describe our improved version of an *Ae. aegypti* weather-driven population dynamics model, ii) compare simulation results with field data and iii) introduce the implementation of the model as part of a stand-alone operational application based on open source software and open access global weather data for those in charge of vector borne diseases surveillance and control. We understand that all of these properties are important: free so that everyone can access and experiment with it; open-source so that it can be examined and validated; stand-alone to automatically retrieve all needed input, run a simulation and show results without any need for extra data sources.

2. Materials and methods

2.1. Model general overview

The original model proposed by Otero et al. Otero et al. (2006) was built for temperate climates under the assumption that rainfall is regular. Population is divided in five compartments, eggs (E), larvae (L), pupae (P), non-parous (A_1) and parous adult females (A_2) (Fig. 1). The evolution of these populations is affected by the events: egg hatching, pupation, adult emergence, completion of gonotrophic cycles and mortality at each stage. The development rate for egg hatching, pupation, adult emergence and completion of gonotrophic cycles are based on the thermodynamic model developed by Sharpe and DeMichele Sharpe and DeMichele (1977). The distinction between non-parous and parous adult females is made because the gonotrophic cycle for the first oviposition takes longer than the subsequent ovipositions (Otero et al., 2006). Furthermore, as in the original model, we assumed that the availability of blood meals for adult females is not a limiting resource.

However, this model makes significant amendments to the original model, which assumed fixed breeding sites, and rainfall-independent hatching. The minimalist nature of Otero et al. Otero et al. (2006)'s model makes it an excellent base to build extended models from, such as the one presented here. Thereby, and to overcome these limitations already described by Otero et al. Otero et al. (2006), we included rainfall and explicitly modeled the amount of water in containers of adjustable size, allowing to introduce precipitations as a trigger for egg hatching. Overall, our model is:

- compartmental: the population is divided according to the observable mosquito life stages (the model considers the full population as a genetically homogeneous set, and it does not account for cohorts),
- deterministic: it represents the average behaviour of the population,
- climate-driven: the population dynamics are mainly driven by temperature and precipitation. The former affects development rates and mortality at certain stages (Christophers, 1960; Focks et al., 1993; Otero et al., 2006) as well as females' gonotrophic cycle (Carrington et al., 2013; Goindin et al., 2012; Marinho et al., 2016) and the latter,

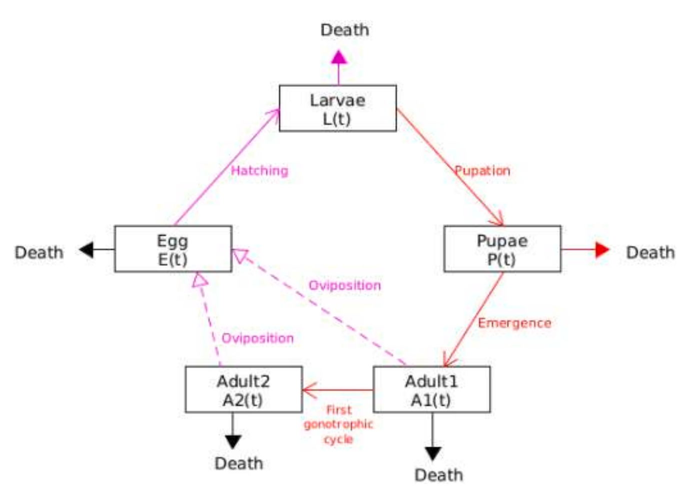

Fig. 1. *Aedes aegypti*'s life cycle. The population stages are indicated in boxes. The arrows indicate transition from one stage to the other. The dashed arrows indicate one stage modifying the other. Processes influenced by temperature are in red and processes influenced by temperature and precipitation are shown in magenta. (For interpretation of the references to colour in this figure legend, the reader is referred to the web version of this article.)

creates (new) potential breeding sites and triggers egg hatching, i.e., eggs submergence is a necessary Christophers, 1960.

- dynamic: most of the events mentioned at the beginning of this section happen at rates that depend on temperature and/or precipitation, which are functions of time since they change during the year. Therefore, the dependence on temperature and precipitation introduces a time dependence to the model.

2.2. Description of Aedes aegypti population dynamics model

The population dynamics model is based on a system of ordinary differential equations (ODE).

The equations read as follows:

$$\begin{aligned}\frac{d\mathbf{E}_{i,j}(t)}{dt} &= egn\ \left(ovr_1(t)\ A_1(t) + ovr_2(t)\ A_2(t)\right)\ \mathbf{ovsp}_{i,j}(t)\ + \\ &-me\ \mathbf{E}_{i,j}(t)\ + \\ &-elr(t)\left(1-\gamma\left(\vec{L}_j(t),\vec{W}_j(t)\right)\right)\ \mathbf{E}_{i,j}(t)\ \mathbf{wm}_{i,j}(t)\end{aligned} \tag{1}$$

$$\begin{aligned}\frac{d\vec{L}_j(t)}{dt} &= elr(t)\ \left(1-\gamma\left(\vec{L}_j(t),\vec{W}_j(t)\right)\right)\sum_{i=1}^{m}\left(\vec{E}_{i,j}(t)\mathbf{wm}_{i,j}(t)\right)\ + \\ &-ml(t)\ \vec{L}_j(t) - \vec{m}dl_j(t)\ \vec{L}_j(t)\ -\ \vec{\alpha}_j\vec{L}_j(t)\ \vec{L}_j(t)\ + \\ &-lpr(t)\ \vec{L}_j(t)\end{aligned} \tag{2}$$

$$\frac{d\vec{P}_j(t)}{dt} = lpr(t)\ \vec{L}_j(t) - mp(t)\ \vec{P}_j(t) - par(t)\ \vec{P}_j(t) \tag{3}$$

$$\begin{aligned}\frac{dA_1(t)}{dt} &= \left(\sum_{j=1}^{n} par(t)ef\frac{\vec{P}_j(t)}{2}\right) - maA_1(t) + \\ &-ovr_1(t)A_1(t)\end{aligned} \tag{4}$$

$$\frac{dA_2(t)}{dt} = ovr_1(t)\ A_1(t) - ma\ A_2(t) \tag{5}$$

The functions and parameters of the *Ae. aegypti* model are described in Table 1 and Table 2, where some values and definitions correspond to the original model presented by (Otero et al., 2006), and new parameters and functions are explained in the text.

Table 1
Functions of the population dynamics model for *Ae. aegypti*.

Function	Description	Reference
$T(t)$	Temperature (K)	
$elr(t)$	Egg hatching rate (day^{-1})	(Otero et al., 2006)
$lpr(t)$	Larval development rate (day^{-1})	(Otero et al., 2006)
$par(t)$	Pupal development rate (day^{-1})	(Otero et al., 2006)
$ovr_1(t)$	Gonotrophic cycle coefficient (number of daily cycles) for adult females in stage 1 (A_1) (day^{-1})	(Otero et al., 2006)
$ovr_2(t)$	Gonotrophic cycle coefficient (number of daily cycles) for adult females in stage 2 (A_2) (day^{-1})	(Otero et al., 2006)
$ml(t)$	Larval mortality (day^{-1})	(Otero et al., 2006)
$mdl(t)$	Larval mortality by desiccation (day^{-1})	Eq. 10
$mp(t)$	Pupal mortality (day^{-1})	(Otero et al., 2006)
$\gamma(L)$	Hatching inhibition by larvae	(Otero et al., 2006)
$ovsp(t)$	Oviposition site preference	Eq. 7
$wm(t)$	Water mask (submerged eggs)	Eq. 8

Table 2
Parameters of the population dynamics model for *Ae. aegypti*.

Parameter	Description	Value	Reference
egn	Number of eggs laid per oviposition	63	(Otero et al., 2006)
me	Egg mortality (day^{-1})	0.01	(Otero et al., 2006)
ef	Emergence factor	0.83	(Otero et al., 2006)
ma	Adult mortality (day^{-1})	0.09	(Otero et al., 2006)
$mdlr$	Larval mortality rate on dry container (day^{-1})	2	To the best of our knowledge
C	Containers		This work
n	Type of containers		This work
Clh	Container Level Height ($cm.$)	0.1	This work
$\vec{\alpha}$	Larval density-dependent mortality ($larvae^{-1}\ day^{-1}$)		(Otero et al., 2006)
$\vec{C}h$	Height of the n types of containers ($cm.$)		This work
$\vec{C}r$	Radius of the n types of containers ($cm.$)		This work
$\vec{C}d$	Proportion of the n types of containers		This work

The original model was modified to incorporate precipitation and different types of containers, which vary in height. In the remainder of this subsection, we address the modifications made for each of the above equations. As for functions and constants in the original model please refer to (Otero et al., 2006).

The subscript i is used to denote the water level inside a container and the subscript j to denote the type of container. For example, $\mathbf{E}_{i,j}(t)$ represents the amount of eggs at level i, in a container j at a time t. As for the units, height/distance is in centimeters, and time in days.

In Eq. (1), $\mathbf{E}(t) \in \mathbb{R}^{m\times n}$ represents the eggs at a time t, in n types of containers, where each type of container is divided in m levels. $n, m \in \mathbb{N}$ are fixed values provided by the configuration of the model.

The breeding site preference $\vec{b}sp$ considers the proportion of eggs laid in each type of container,

$$\vec{b}sp_j(t) = \frac{W_j(t)}{W_j(t)+\varepsilon}\ \vec{C}d_j \tag{6}$$

where Cd_j is the proportion of containers of type j, $\vec{W}_j$ is the water level (in cm) in a container of type j and $\varepsilon = 0.0001$. A container with water is suitable for the adult female to lay eggs while dry containers are not eligible for oviposition. Hence, the function $\vec{b}sp_j(t)$ must differentiate a dry container from a container with water. To achieve this we use $\frac{W_j(t)}{W_j(t)+\varepsilon}$ as an approximation of a step function that is 1 when the water level is greater than 0 and 0 when the container is dry. The smaller the value of ε, the closer the approximation. The value for ε was set arbitrarily, but aims to obtain a low sensitivity(2.8). We followed this approach to avoid artifacts in the solution.

Eggs are usually laid on the sides of the container just above water level (Christophers, 1960). Hence, we consider the function Oviposition Site Preference (ovsp)

$$\mathbf{ovsp}_{i,j}(t) = \begin{cases} \dfrac{\vec{b}sp_j(t)}{max\left(\sum_{j=1}^{n}\vec{b}sp_j(t),\varepsilon\right)} & if\ \ Clh\ \ (i-1) \le W_j(t) < Clh\ \ i \\ 0 & otherwise \end{cases} \tag{7}$$

where Clh is the level height, a constant defined in the configuration file. The accuracy of the position where eggs are laid within the breeding site (i.e., a level) is determined by Clh. The smaller the level height, the more levels each container will be divided in. The fraction in 7 is used to consider the proportion of available breeding sites only. The *max* function is used to avoid numerical issues when $\overrightarrow{b}sp_j(t)$ is close to 0 for all container types at the same time.

We assume that eggs need to be submerged in order to hatch (Christophers, 1960). The function Water Mask (*wm*) is used to select eggs below water level only,

$$\mathbf{wm}_{ij}(t) = \begin{cases} 1 & if \;\; Clh \;\; (i-1) \leq W_j(t) \\ 0 & otherwise \end{cases} \tag{8}$$

Livdahl et al. Livdahl et al. (1984) found that a high density of larvae can prevent eggs from hatching. To include this phenomena, Otero et al. Otero et al. (2006) introduced the γ function. This function was slightly modified here to take into account the amount of water in a cylindrical container of fixed radius $\overrightarrow{C}r_j$. If there is no water, the hatching is totally inhibited. When the container is filled, if larval density is less than the threshold, no inhibition takes place, but when the density surpasses the threshold, partial inhibition occurs.

$$\gamma\left(\overrightarrow{L}_j(t), \overrightarrow{W}_j(t)\right) = \begin{cases} 1 & if \;\; \overrightarrow{W}_j(t) \leq \varepsilon \\ 0 & if \;\; \overrightarrow{W}_j(t) > \varepsilon \;\; and \;\; \dfrac{\overrightarrow{L}_j(t)}{C \;\; \overrightarrow{C}d_j} \leq a_0\left(\overrightarrow{W}_j(t), \overrightarrow{C}r_j\right) \\ 0.63 & otherwise \end{cases} \tag{9}$$

where $a_0\left(\overrightarrow{W}_j(t), \overrightarrow{C}r_j\right) = 70 \;\; \overrightarrow{W}_j(t) \;\; \pi \overrightarrow{C}r_j^2 \;\; 10^{-3}$. The critical density, 70 larvae per litre, is the density where the hatching fraction changes. Otero et al. Otero et al. (2006) considers critical density values between 10 and 70 larvae per litre. In a later work, however, the inhibition of egg eclosion due to high larval density was no longer considered because it was not observed in field studies (Otero et al., 2008). While we kept the effect of inhibition, the highest critical density was used to reduce its influence. Concisely, hatching depends on temperature by the *elr*(*t*) function, on larval density by the function γ and on water level by $\mathbf{wm}_{i,j}(t)$.

In Eqs. (2) and (3), $\overrightarrow{L}(t), \overrightarrow{P}(t) \in \mathbb{R}^n$ represent larvae and pupae in n types of containers at time t. We consider an increment of larval mortality in the event of a container drying out (i.e., mortality caused by desiccation):

$$\overrightarrow{m}dl_j(t) = mdlr \;\; \left(1 - \frac{\overrightarrow{W}_j}{\overrightarrow{W}_j + \varepsilon}\right) \tag{10}$$

where $mdlr = 2 \;\; day^{-1}$ (Table 2) is a constant estimated to the best of our knowledge.

In Eqs. (4) and (5), $A_1, A_2 \in \mathbb{R}$ represent nulliparous and parous adult females. The first equation was slightly modified to take into account the adult females emerged from several types of containers, and the second equation remained unchanged from the original model. $\overrightarrow{W}$ represents the amount of water in the n types of containers. For example, $\overrightarrow{W}(t) = (1.5, 3.2)$ indicates that at a time t, the containers of type 1 contain 1.5 cm of water, and containers of type 2, contain 3.2 cm.

The water is incorporated (Quantity Gathered) through precipitation, $QG(t) = p(t) \;\; 10^{-1}$. To account for water lost by evaporation (Quantity Released), the Ivanov model is used (Romanenko, 1961) with temperature expressed in Kelvin.

$$QR(t) = 6 \;\; 10^{-5} \;\; (25 + T(t) - 273.15)^2 \;\; (100 - RH(t)) \;\; 10^{-1} \tag{11}$$

Let us consider $\widetilde{W}_j$ by solving

$$\frac{d\widetilde{W}_j(t)}{dt} = QG(t) - QR(t) \tag{12}$$

To obtain $\overrightarrow{W}_j$, this expression was slightly changed to contemplate the fact that $0 \leq \overrightarrow{W}_j \leq \overrightarrow{C}h_j$ where $\overrightarrow{C}h$ consists on the height of the n types of containers. Other approaches to take rainfall into account can be found in (Aznar et al., 2013; Gong et al., 2010; Lee et al., 2016; Tran et al., 2013; Valdez et al., 2017).

Precipitation is obtained as a set of discrete daily values. Since it is convenient to work with a continuous function, $p(t)$ was introduced and constructed as follows: Let $\overrightarrow{P} := (P_0, \dots, P_{l-1}) \in \mathbb{R}^l$ be the vector of daily accumulated precipitations, where the precipitation rate $p(t) : \mathbb{R} \to \mathbb{R}$ is:

$$p(t) = P_{\lfloor t \rfloor}\left[sin\left(2\pi t + \frac{3\pi}{2}\right) + 1\right] \tag{13}$$

and $P_{\lfloor t \rfloor} \in \{P_0, \dots, P_{l-1}\}$. An example of the function $p(t)$ is shown in the supplementary material. The motivation behind $p(t)$ was to build a simple continuous function in which the area under the curve, for any given day, is equal to the accumulated precipitation for that day. For $T(t)$ and $RH(t)$ functions, a one-dimensional interpolating spline from Python's SciPy package (Jones et al., 2001) was used.

2.3. Model initial conditions and simulations

The equations were solved numerically using the Runge-Kutta (RK4) method implemented in C++17, with a time step $h = \frac{1}{20}$. The simulations were run for the period 2015–2020, with an initial population of 100 eggs and one ideal cylindrical container. Parameters took the following values $C = 1, n = 1, \overrightarrow{C}r = 5, \overrightarrow{C}d = 1$. The value for *Ch* will be explicitly mentioned for each simulation.

2.4. Model implementation within a software application

The *Ae. aegypti* model was implemented as a module in a larger software application that also retrieves the meteorological data, needed by the model, and presents the output as a plot of mosquito abundance per life stage over time. A block diagram of the application that we developed is outlined in Fig. 2. The *get_weather* module automatically downloads meteorological datasets (See section 2.5) and transforms the original GRIB or NETCDF formats into a.csv time series for the coordinates defined in the get_weather.cfg configuration file of the application. This configuration file is a list of cities with their latitude and longitude coordinates. The file is then parsed and processed resulting in a time series.csv for each city in the list. The module was implemented in Python 3 using *pygrib* v2.0.2, *netCDF4* v1.5.3 and the standard multiprocessing package to extract several points simultaneously. The application produces the output in.csv format or as an interactive plot in. html format. This output contains mosquito population values per stage and water level at each time step.

The source code of the application is available at *https://github.com/CONAE-GVT/aedes_aegypti/tree/master*. The implementation can be found at http://pluton.hopto.org:8080/app.

2.5. Meteorological input data

The *Ae. aegypti* model uses three meteorological variables: daily mean temperature, daily mean relative humidity and daily accumulated rainfall. These variables are obtained from the National Oceanic and Atmospheric Administration(NOAA, 2021), the National Aeronautics and Space Administration (NASA (NASA, 2021)) and the University Corporation for Atmospheric Research (UCAR (UCAR, 2021)) (Table 3:). The advantage of using these sources is the availability of data in areas with no close-by weather stations. Moreover these datasets are global and completely free.

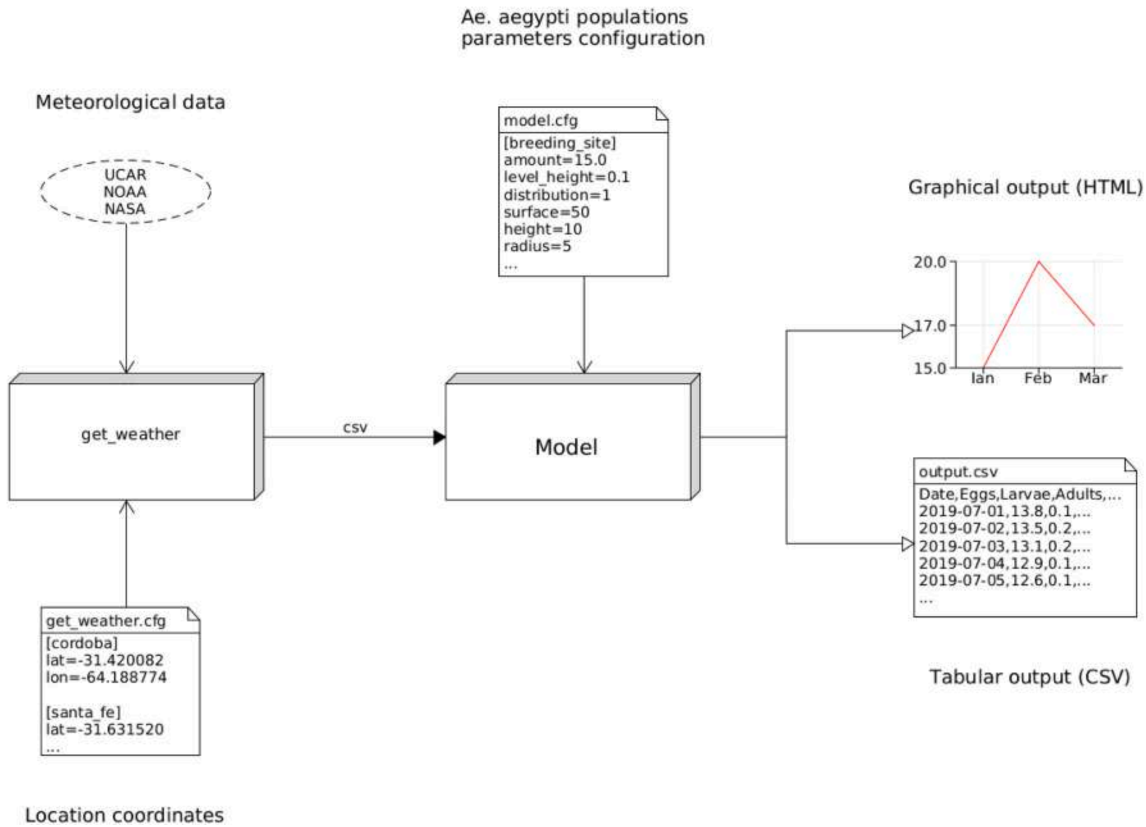

Fig. 2. Diagram of the application. The get_weather module downloads meteorological data and produces time series in.csv format. The time series are ingested by the model and the simulation results are exported as an.html dynamic curve or.csv data.

Table 3
Meteorological Sources. The National Centers for Environmental Prediction Final Analysis (NCEP-FNL) is a data product from the Global Data Assimilation System (GDAS), which continuously collects observational data from the Global Telecommunications System (GTS), and other sources.

Variable(s)	Source	Description	Dataset	Grid Resolution
Historic Temperature Relative Humidity	UCAR	Full period	NCEP GDAS/FNL	0.25°×0.25°
Historic Temperature Relative Humidity	NOAA	Daily	NCEP GDAS/FNL	0.25°×0.25°
Historic Precipitation	NASA	Daily	GPM_3IMERGDL	0.1°×0.1°
Forecast Temperature Relative Humidity Precipitation	NOAA	Daily	NCEP CFS Forecasts - Flux, NCEP CFS Forecasts - Pressure	1°×1°

The Global Precipitation Measurement (GPM) is an international satellite mission to provide observations of rain worldwide. The Integrated Multi-satellitE Retrievals for GPM (IMERG) is the unified algorithm that provides rainfall estimates combining data from all passive-microwave instruments in the GPM Constellation. The Daily Late (DL) run dataset is used.
The Climate Forecast System (CFS) is a fully coupled atmosphere–ocean–land model used at NCEP for seasonal prediction.

2.6. Entomological validation data

The output of the model was compared with surveillance data obtained by Córdoba's Health Ministry. Córdoba is the second largest city in Argentina, with a surface of 576 km^2 and a population of about 1.3 million inhabitants (INDEC, 2010). The climate is temperate with a mean annual temperature of 17.4 °C and a mean annual rainfall of 738 mm (Fig. 6).

Ovitraps are among the standard methods used to detect the presence and monitor the activity of *Ae. aegypti* (Schweigmann et al., 2002). In our study, the field data used for validation corresponds to 300 ovitraps placed in 150 house gardens over the city of Córdoba (Andreo et al., 2019). The surveillance was carried out weekly from October 2017 to January 2020 by the Health Ministry. Importantly, the ovitraps placed in each house are not discriminated, i.e., they are not labelled A and B; so we used the average number of eggs from the two ovitraps placed in each house to compare with the model's output. The latter is calculated as:

$$\frac{d\mathbf{O}_{i,j}(t)}{dt} = egn\ \left(ovr_1(t)\ A_1(t) + ovr_2(t)\ A_2(t)\right)\ \mathbf{ovsp}_{i,j}(t) \tag{14}$$

A similar approach can be found in the work developed by Tran et al. Tran et al. (2013).

Two widely used measures of time series proximity are the Euclidean distance and dynamic time warping. These two focus on the closeness of values disregarding similarity of growth behaviour. Instead, we used the dissimilarity index D presented by Chouakria and Nagabhushan Chouakria and Nagabhushan (2007) because it takes into account both, behaviour and values' proximity. For two time series S_1 and S_2, D is defined as: $D(S_1,S_2) = f(cort(S_1,S_2))\ \ \delta_E(S_1,S_2)$ where $f(x) = \frac{2}{1+e^{kx}}$, where $k \geq 0$, *cort* is the temporal correlation and δ_E is the Euclidean distance (Chouakria and Nagabhushan, 2007).

The dissimilarity index was used to assess the proximity between simulations and field data and, also, between simulations obtained with observed vs forecasted weather data. See section 3.2 for a detailed explanation along with the results.

2.7. Simulations for different geographic locations

Besides Córdoba, we selected four other cities, located in different biogeographical regions of Argentina (Burkart et al., 1999), to run simulations. Two of these are located in the southern limit of *Ae. aegypti* distribution. We ran simulations using meteorological data of those locations to compare the model behaviour and model output under a wide range of environmental conditions. The temperature increases from Bahía Blanca to Tartagal (south to north); and precipitation decreases towards west. The cities and their climate characteristics are summarized in Table 4.

2.8. Sensitivity analysis

2.8.1. Initial conditions

We compared simulations with different initial values for the egg population. A similar approach can be found in Otero et al. Otero et al. (2006).

2.8.2. Parameters

We performed a one-way sensitivity analysis on the model by varying a $\pm$25% of the baseline values of individual parameters one at a time (all the rest constant) in order to analyze their individual impact on the maximum abundance of adult females A_{max} for Córdoba city from October 2017 to January 2020 with an 8 cm container. A similar approach can be found in Valdez et al. Valdez et al. (2017).

2.8.3. Temperature and precipitation

The *get_weather* module generates a time series csv with temperature in degrees Celsius (converted to Kelvin) and precipitation in millimeters (converted to centimeters) for model input. We analyzed the impact of weather variables on the maximum abundance of adult female mosquitoes A_{max} for Córdoba from October 2017 to January 2020 with 8 cm containers by varying *pm*5% temperature and precipitation in the time series csv.

3. Results

3.1. Aedes aegypti population dynamics

We present here the outputs of our mechanistic model based on meteorological data acquired for Córdoba city. The predicted abundances for each mosquito life stage are reported in Fig. 3, where the abundance values are represented for one putative container of 10 cm height ($Ch = 10$). The general pattern shows activity onset by October and the annual peak by the end of February. The egg counts increased later than the other stages, since only already developed adult females are able to lay eggs. Eggs reached the peak in April with variable maximum values: 200 eggs in 2018, 700 in 2019 and 450 in 2020 (eggs are scaled down by a factor of 10^{-2} to be shown alongside water content).

Table 4
Biogeographical summary of the locations simulated.

City	Eco-region	Mean AT	Rainfall	Climate
Tratagal	Yungas/ Mountain Forest	14–26 °C.	900–2.500 mm.	Warm and humid
Bahia Blanca	Espinal	15–25 °C.	340–1170 mm.	Warm and humid at north, temperate and dry to south
Santa Fe	Espinal			
Córdoba	Espinal/Dry Chaco			
Gral Roca	Plains and plateau	13–17 °C	80–300 mm.	Temperate Dry

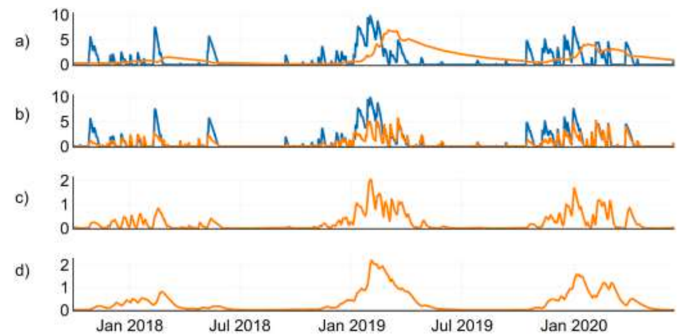

Fig. 3. Mosquito population dynamics simulated for different life stages using meteorological data for Córdoba city. (a) Eggs x 10^{-2}, (b) Larvae, (c) Pupae, (d) Adult females. Orange lines represent the number of individuals yielded by a container of 10 cm height. Blue line represents simulated water content in cm. (For interpretation of the references to colour in this figure legend, the reader is referred to the web version of this article.)

The more variable larvae and pupae populations reflect the effect of water amount in each container (blue line, in Fig. 3). As a reference, when water content varies intermittently between 0 and 4 cm (from October to December 2019), the larval counts remain low. When water content goes to zero, as in March 2019, the larval population also goes down. Larval density dependent mortality included in eq. 2, constrains the maximum value fluctuating around 5 larvae per container, even when water content is not limiting.

The adult population varies in a smoother way and with low individual counts, denoting the competitive environment for immature stages within each container. In the last warm period (November 2019 to March 2020), the model output shows a curve with a marked increase of larvae and the maximum number of adult females on November 15. Meanwhile, this adult count was reached 25 days later, on December 11 in the previous year (November 2018 - to March 2019). In both warm periods, the curves decline by mid-April, but densities greater than zero adult females per container are observed until mid-May. This is in accordance with the timing of the largest Dengue outbreak in Córdoba history, with active notification of human cases until early June 2020 (Córdoba Epidemiological Report, 2020).

3.2. Predictions with forecast meteorological data

The model takes input from observed or forecast meteorological data to make predictions after the simulation date. An approach to assess the model accuracy, when using forecast data, is shown in Fig. 4a.

Fig. 4a shows the simulated number of adult females from 7 January 2019 to 4 February 2019 using either forecast or observed meteorological data as input. The black line is obtained running the model with only forecast data as input and the magenta line is obtained using observed meteorological data, i.e., it simulates/predicts for observed weather conditions. In order to compare the different outputs in Fig. 4a, we used the dissimilarity index D, $D_i = D(S_M, S_i)$, where "M" is the total amount of simulation dates and "i" is the amount of days from the initial date when each simulation was ran. The value "i" can be also seen as the amount of days of observed meteorological data used by each simulation. This is shown in Fig. 4b, where the lower the D value, the better the accordance between the curves. As it can be seen, D has a peak at day 20, and then remains low until until day 28. This pattern is more evident in 4c, where D is obtained as an average of 55 time windows. After 15 days of forecasted data, the mean D measure increases above 0.5 as well as its variation.

3.3. Comparison with field entomological data

The model output, specifically the number of eggs, was compared

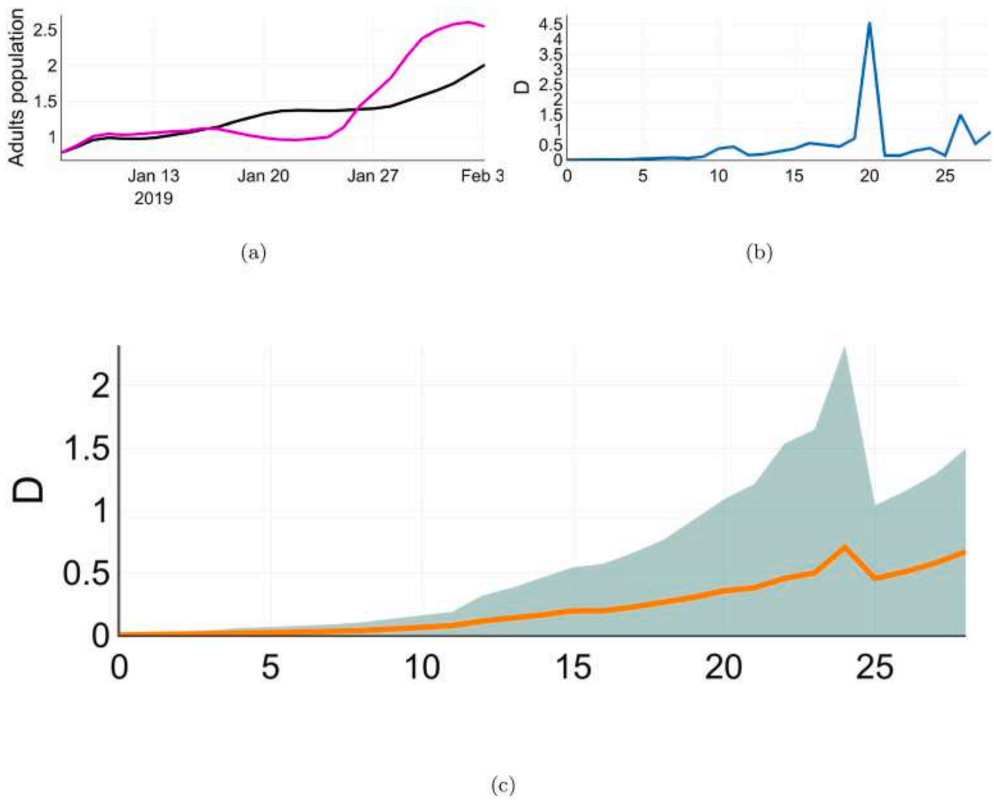

Fig. 4. (a) Number of adult females for one container of 10 cm height located in Córdoba from 7 January 2019 to 4 February 2019. In magenta: the result of the model ran with input data composed solely of observed meteorological data; in black: the result of the model ran with input data composed solely of forecast meteorological data. (b) The dissimilarity index D computed between the model's output using solely observed meteorological data and the model's output using x days of forecast is shown for the period 7 January 2019 to 4 February 2019. On the x axis we represent the amount of forecast days used by the model. (c) The procedure in (b) is repeated for 55 time windows between September and June, within the period December 2018–February 2021. The mean D curve (in orange) ± SD (light green area) is shown. (For interpretation of the references to colour in this figure legend, the reader is referred to the web version of this article.)

with entomological data of the oviposition surveillance carried out by the Córdoba Health Ministry as described in section 2.6.

To evaluate the model performance, the weekly oviposition was simulated for containers of 1, 3, 6, 8 and 10 cm height from October 2017 to January 2020. Then, D was calculated for 5 heights and 150 locations. Most of the ovitraps time series had a better accordance with the model outputs for a 3 cm height container, with a mean value and standard deviation of the dissimilarity index, D, of 252 ± 119, while containers of 1, 6, 8 and 10 cm height had a mean value of 278 ± 179, 374 ± 141, 405 ± 157 and 448 ± 165, respectively.

Ovitraps placed in the South West and North West of Córdoba city showed in general, better accordance with the model output for a 3 cm height container, with a mean value of 232 ± 123 and 225 ± 104, respectively.

In Fig. 5 we compare the simulated oviposition with the collected field data from a particular house. The houses were selected on the basis of the lower D values (see above) only for graphical comparison purposes. A 1 cm height container will dry out more frequently than those of greater height, so the oviposition will vary more, as can be observed in Fig. 5a between January 2019 and April 2019. It is important to notice that the container's height affects not only oviposition values (expressed as weekly number of eggs per container) but also the timing of the maximum egg count. For the case of 1, 3, 6, 8 and 10 cm height containers simulations, the maximum weekly oviposition increases and the date of the maximum oviposition is delayed proportionally with container height. For a 1 cm height container, the maximum value is 108.5 eggs and was observed on 3 February 2019; a 3 cm height container, the maximum value is 186.1 eggs and was observed on 3 February 2019; for a 6 cm height container the maximum is 265.9 on 11 February 2019; for a 8 cm height container the maximum is 312.4 on 24 February 2019 and for a 10 cm height container the maximum is 334.6 on 24 February 2019. This figure also shows to what extent the model predictions are in accordance with four ovitraps in terms of oviposition onset and offset, maximum value and maximum oviposition date. Simulated dynamics for a 10 cm container compared to the mean number of eggs collected by the 150 pairs of ovitraps are shown in Fig. 5e.

3.4. Simulations for different climates

The model's outputs for different cities in Argentina are shown in Fig. 6. Córdoba and Santa Fe, located in temperate climates, show a fluctuating pattern where *Ae. aegypti* populations drop during winter and only eggs overwinter. Both cities show an increase in egg numbers from 2018 to 2019 (also observed with field data in Córdoba); but in Tartagal (Yungas region), the model predicts a higher peak during the 2018 warm season. In the more humid cities (Santa Fe and Tartagal), the number of eggs predicted is clearly higher and the oviposition activity (with more than 10 eggs per breeding site) is extended until mid-June, while in driest cities it decreases earlier. General Roca and Bahía Blanca, are the driest and coldest cities considered (located at the austral limit of *Ae. aegypti*). Bahía Blanca showed between 15 and 20 times less eggs than Tartagal and Santa Fe, while no eggs were documented in General Roca during the period simulated. These simulated outputs, suggest that the presence of Dengue vector is really constrained by weather at these southern locations.

3.5. Sensitivity of model outputs

Simulations with different initial values show little impact in the population numbers of subsequent years (Fig. 7). All the simulations in the present study start on 20 July 2015, but a window is retained for output computation or presentation. For example, in Fig. 7 the window from Oct 2015 to June 2020 is shown.

We examined all parameters in Table 2. The results are summarized in Table 5. The first five parameters have a strong influence on the maximum adult female abundance. As expected more containers have a direct impact on A_{max}. The remaining parameters showed weaker influence on the model's output.

The impact of temperature and precipitation is summarized in

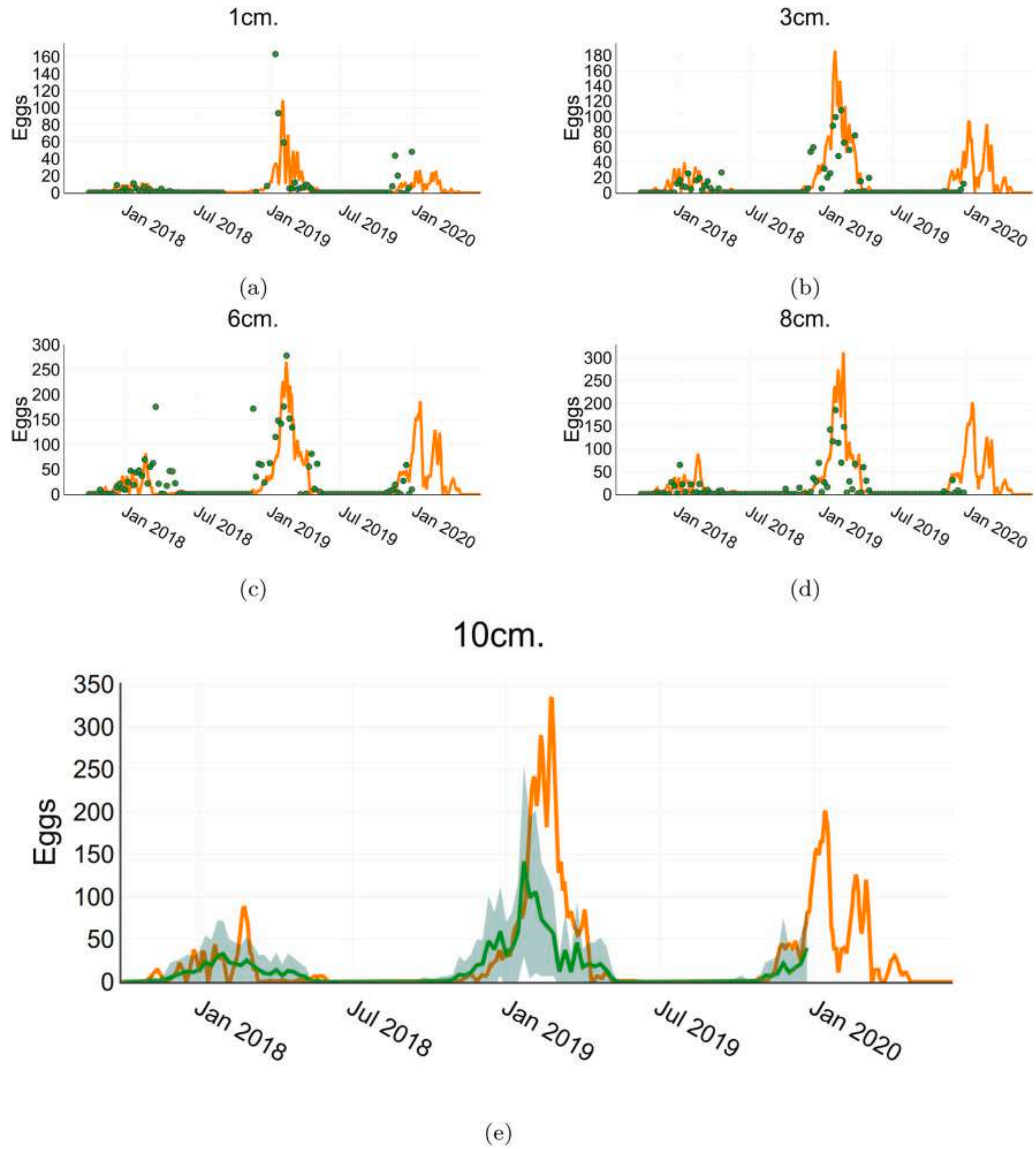

Fig. 5. Simulated weekly oviposition for containers of 1, 3, 6 and 8 cm height from October 2017 to June 2020 (in orange) were compared to the mean number of eggs collected per ovitrap in four different households in Córdoba city (green). The fifth plot corresponds to a simulated dynamics for a 10 cm height container (in orange) compared to the mean number of eggs collected by the 150 pairs of ovitraps (in green) and their standard deviation (light green area). (For interpretation of the references to colour in this figure legend, the reader is referred to the web version of this article.)

Table 6, where a strong influence of temperature is observed.In contrast, precipitation showed lower influence over adult female abundance when all other parameters remain unchanged.

4. Discussion and conclusions

Here, we present an enhanced version of a classical mechanistic model of *Aedes aegypti* population dynamics, driven by two variables: temperature and precipitation. Designed to work with public weather databases, it describes the mosquito life cycle in five different stages (egg, larvae, pupae, young adult females and adult females after first oviposition). Our model includes a number of improvements and innovations over previous existing variants, namely: the effect of precipitation on egg hatching and increase in larval mortality in the event of a container drying out, the explicit modeling of container type and container features, as well as the amount of water in a container. The weather data source is a key aspect of the application which is designed to work with remotely sensed and gridded data. This allows the execution of the model for any pair of coordinates, whether there's a weather station in close proximity or not. With this improvement, we solve a challenge presented when using previous *Ae. aegypti* population dynamics models (Aznar et al., 2013; Ellis et al., 2011; Lana et al., 2014; Otero et al., 2006).

Initially conceived to respond to a specific request from Córdoba zoonoses program, the population dynamics model is embedded into a system that allows users to set coordinates for input weather data at any place or city. Moreover, the model allows users to obtain forecasts of *Ae. aegypti* population density curves by inserting forecasted weather data as

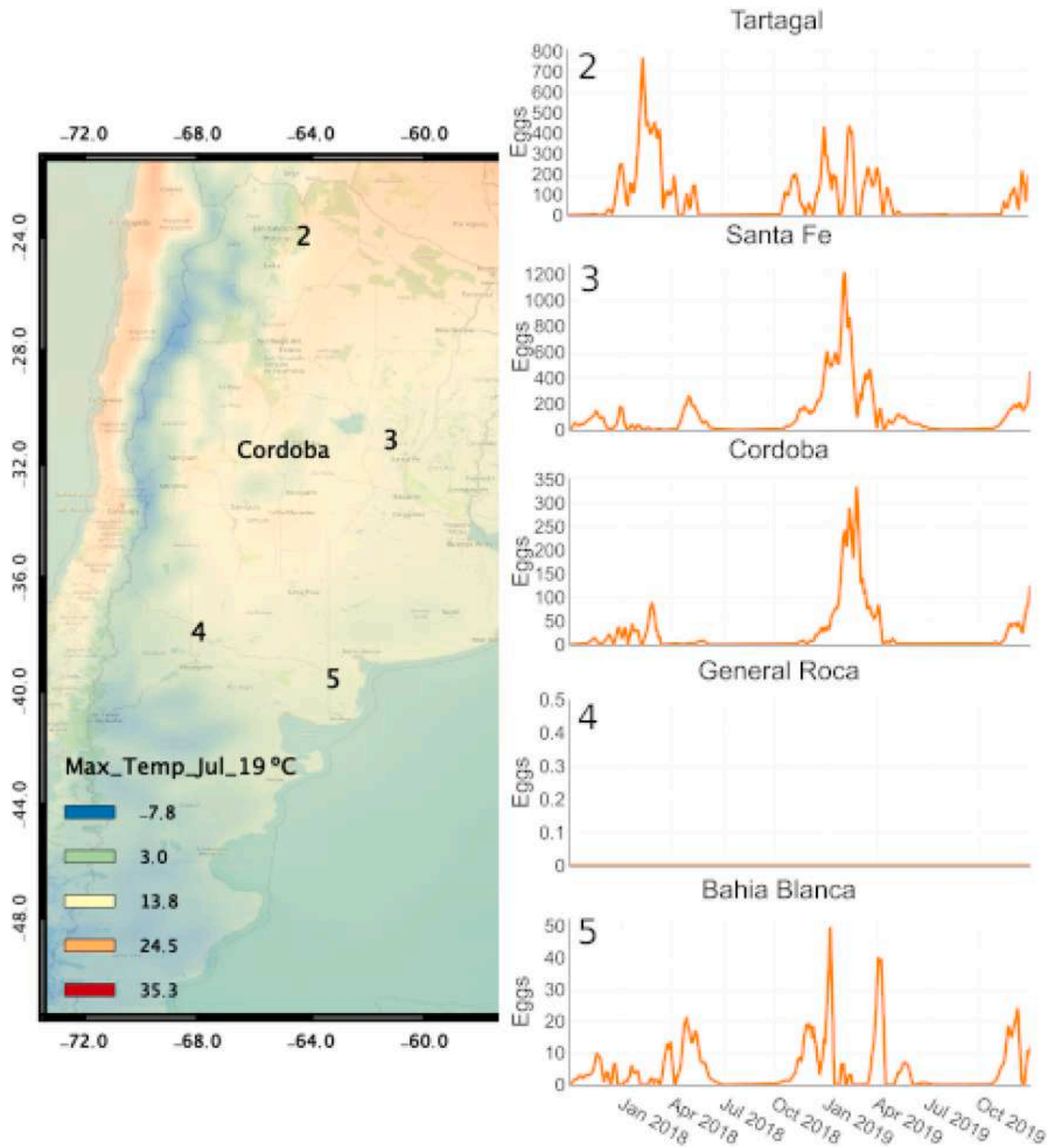

Fig. 6. Simulated dynamics of accumulated eggs laid over a week at time t based on meteorological data from 2018 to 2019. Outputs for different cities in Argentina: 2) Tartagal, 3) Santa Fe, 4) General Roca, 5) Bahía Blanca. Background image corresponds to July mean temperature (ISAGRO geo-server (ISAGRO, 2021)).

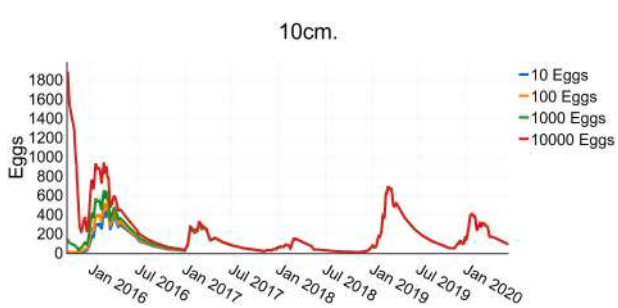

Fig. 7. Sensitivity analysis. Simulations with different initial egg numbers over four years time. Outputs show no strong sensitivity when the next favourable cycle occurs.

Table 5
Sensitivity analysis. Each parameter in the first column was modified, one at a time, increasing or decreasing its value by 25%. The percentages in the second and third column represent the effect on adult females abundances.

Parameter	−25%	25%
ef	−46%	60%
ma	51%	−29%
$\vec{\alpha}$	33%	−20%
egn	−28%	28%
C	−25%	25%
me	5%	−5%
$\vec{C}h$	−4%	3%
mdlr	1%	−1%
Clh	−1%	1%
$\vec{C}r$	−1%	0%
ε	1%	−1%

Table 6
Sensitivity analysis. Temperature and precipitation were modified, one at a time, increasing or decreasing its value by 5%. The percentages in the second and third column represent the effect on adult females abundances.

Parameter	−5%	5%
Temperature	−35%	47%
Precipitation	−5%	5%

input. Hence, the proactive model serves as a decision-making program, like those recommended by WHO WHO (2010).

Our data from Córdoba City showed that the model outputs, generated from forecast weather, are reliable up to 15 days in advance, with low divergence from observed population curves (Fig. 4c). A period of 15 days is long enough to advice and plan different control actions for effective prevention of arboviral disease outbreaks. Furthermore, the system can generate outputs in an easily visible format, such as the.html dynamic curve or as.csv data for further external processing. Among model outputs, the temporal variation of water content in the breeding site, for example, allows users to hypothesize the productivity of different types of containers (i.e., putative adult females' yield as a function of water content variation over time, considering the shape of the container).

Oviposition data (number of eggs) collected weekly shows great variability. The results of the simulations for 2018 and 2019 were consistent with the number of eggs collected in certain ovitraps in the city of Córdoba. A significant increase was observed for summer 2019 with respect to the previous year in both field data and simulated data. As general pattern, the model reported a great accordance with those field data series displaying higher abundance (Andreo et al., 2019). Different levels of accordance were observed between simulated and observed data considering major spatial quadrants of the city (North, West, South, East and Center). However, as the objective of this work was moreover to describe (in advance) the general environment of a city, or other administrative unit under the same vector control strategy/policy, we did not test fine spatial resolution environmental variability. Notwithstanding, to explain the variability of field data, the heterogeneous (micro) habitats that can be found in a city should be considered. In that direction, and following Landscape Epidemiology principles some preliminary works used optical images to map this spatial variability and predict Dengue risk in Córdoba city (Rojas et al., 2017; Rotela et al., 2017; Scavuzzo et al., 2018). In the near future, we plan to spatially extend our model by adjusting model parameters such as proportions of containers in order to represent the different dynamics of individual ovitraps in the field.

Although the model was validated with field data from Córdoba city only, the outputs ran in different localities of Argentina showed an overall accordance with *Ae. aegypti* presence at its south-east distribution (Bahía Blanca) (Diaz-Nieto et al., 2013; Rubio et al., 2020b) and with higher abundances expected in the more humid and warmer cities to the north (Tartagal and Santa Fe). Even though the biological parameters of the model are established following existing literature of *Ae. aegypti*'s populations from temperate regions (Francia and Maciá, 2011; Otero et al., 2006), the system allows for parameter modifications (through adjustments in the configuration file and constants in the source code) in order to suit other population conditions. Parameters reflect characteristics of the species and characteristics of the environment, so modifications on these parameters could be required for example due to genetic plasticity in populations (Craig Jr et al., 1961), co-occurrence of *Ae. aegypti* and *Culex* sp. species in breeding sites (Montes et al., 2020) and more; here the most sensitive population parameters in the model were not checked with experimental data. The plasticity of the complete system is in accordance with the multi-scale approach of eco-epidemiologic analysis for vector-borne diseases in changing environment contexts (Chandrasegaran et al., 2020).

As with any model there are a number of limitations and shortcomings that must be acknowledged. Some are related to the type of model, others to the inclusion (or lack of) and estimation of parameters and functions, some might have to do with assumptions made or the effect of driving factors over parameters, etc. Among those related to parameters and functions we can highlight that α, the larval density-dependent mortality, associated with the carrying capacity due to intra-specific competition for food and other resources, was used as in Otero et al. Otero et al. (2006). However, as carrying capacity depends on the environment, this value should be affected by water content (Francia and Maciá, 2011) in future model improvements. In addition, in our current implementation, egg hatching depends only on submergence. We are not considering other biotic factors as bacteria levels, for example, as done by Aznar et al. (2013). Larval food deprivation is not included in the model, but it might have an important role affecting their development rates (Aznar et al., 2013; Romeo Aznar et al., 2018), adult weight (here fixed in 1.35 mg) and therefore oviposition (Bar-zeev et al., 1957; Nayar and Sauerman Jr, 1975). In any case, we do include a coefficient related to larval carrying capacity that might account, at least partially for food availability. Future improvements might include the effects of inter-specific competition, chemical interaction and predation found to be important by Francia and Maciá (2011). Moreover, the use of local studies to estimate the parameters of the development rate functions, instead of those from (Otero et al., 2006), could lead to improved model accuracy. We used here a deterministic model for its simplicity, but if less favourable conditions were to be modeled, possibly leading to species extinction, a stochastic model should be preferred (Aznar et al., 2013; Otero et al., 2006).

Another shortcoming identified is related to the lack of variety in the containers modeled. We assume an ideal cylindrical container. This shape selection was motivated by the information provided by Córdoba's Health Ministry, that reported buckets, bottles and cans as the most common containers found. These are partially in accordance with the preference reported by Otero et al. Otero et al. (2006) and Francia and Maciá (Francia and Maciá, 2011). Furthermore, ovitraps are also cylindrical containers. In any case, it would be relevant for the operational use of this tool, however, to be able to simulate mosquito population evolution for different availability (number and types) of containers such as tyres, for example. Indeed, the breeding site preference function in our model depends on the proportion of containers of a certain type and on the water content in it, but Wong et al. (Wong et al., 2011) found that the choice of an ovipostion site is also influenced by conspecific larvae and pupae. Hence, a more detailed description of containers and the selection process can lead to the simulation of a broader range of scenarios. The addition of indoor containers would be of great relevance too, though the main challenge will be then to estimate indoor temperatures and artificial irrigation. All these possible improvements should be, however, carefully implemented, since, as (Legros et al., 2016) concluded in their analysis, biological assumptions incorporated in models are not always explicit and the structure of the models is not neutral, i.e., it will partly determine the outcome.

Regarding limitations associated with driving factors, the development rates used are valid for temperatures in a range of 4.85–29.85 °C (Sharpe and DeMichele, 1977). This range should be further extended to perform reliable simulations in locations with higher/lower temperatures. Furthermore, we are now considering that the daily mean temperature of containers is equal to the mean daily air temperature. This might have a smoothing effect creating a unrealistically favourable environment. Given how sensitive the model seems to be to temperature changes, we are considering the use of minimum and maximum temperature for further improvements as it was shown that fluctuating temperatures affect *Ae. aegypti* development times and adult sizes (De Majo et al., 2019). In this way, we could also include the deadly effect of high temperatures. Given the geographic expansion of *Ae. aegypti*, a key point is to have life tables of the vector from locations in the limits of its actual distribution. Some field and laboratory studies are now in that direction (Campos et al., 2020; De Majo et al., 2019). In this work, the parameters for the different developmental rate functions were taken from Otero et al. (Otero et al., 2006), and an estimation of these parameter using local studies could lead to a considerable accuracy improvement. Indeed, non linear approximations to fit development rates parameters as function of temperature (such as Briere et al., 1999; Logan et al., 1976; Sharpe et al., 1977) could be tested in the future. Different precipitation rate functions and their effects over model accuracy should be assessed in the future as well as should other sources of weather data of higher temporal resolution to avoid the use of interpolating functions.

Within the present context of the increasing number of Dengue cases at the national and international level (PAHO/WHO, 2020), during summer 2020, Córdoba experienced the largest Dengue outbreak in its history (with more than 2700 cases) (Córdoba Epidemiological Report, 2020). The beginning of oviposition activity as well as its extended duration until the first days of May obtained in advance with the model (3), are useful features to alert about potential outbreaks. Human cases were notified from 14 February 2020 up to mid June (Córdoba Epidemiological Report, 2020), the temporal correspondence between the modeled *Ae. aegypti*'s adult females and human cases is a valuable information, that we aim to analyze shortly. The spread and dynamics of a disease outbreak does not depend only on the vector density. However, the potential of this application can be combined with other vector control data as in the previously implemented system in Argentina (Porcasi et al., 2012), which takes into account temperature, virus circulation, and vector control data, to generate an overall Dengue Risk map. Indeed, the model introduced in this work, complements spatial approximations to map mosquitoes and Dengue risk in different cities of Argentina (Albrieu-Llinás et al., 2018; Espinosa et al., 2016; Porcasi et al., 2019; Rotela et al., 2017; Scavuzzo et al., 2018).

In conclusion, we have accomplished an improved weather-driven population dynamics model for *Ae. aegypti*. Temperature and rainfall data are obtained from open access global weather databases broadly used in early warning systems. We also introduced the implementation of the model as part of a stand-alone operational application based on open source software, so it can be implemented anywhere, regarding the availability of weather stations. Considering the vector modeling, we emphasize the effects of observed rainfall on the physical conditions of potential breeding sites and egg submergence; while temperature was conservatively implemented following previous studies. The final product serves as a plastic tool (i.e., adaptable for biologic parameters and other geographic places), user-friendly tool, that issues quick and proactive outputs, for those in charge of vector borne diseases surveillance and control.

Data statement

The source code is available at https://github.com/CONAE-GVT/aedes_aegypti. The implementation can be found at http://pluton.hopto.org:8080/app. The ovitraps field data is not available since its sensitive information.

Funding

This work was supported by Comisión Nacional de Actividades Espaciales (CONAE), Secretaría de Ciencia y Tecnología - Universidad Nacional de Córdoba (SECyT- UNC) and Ministerio de Salud de la Provincia de Córdoba.

Declaration of Competing Interest

The authors declare no conflicts of interest.

Acknowledgment

The authors acknowledge CONAE and the support given by the Institute of Space Studies"Mario Gulich" (Gulich Institute). The implementation source code is host on github, and was developed by E. Aguirre during his internship in CONAE. We want to thank Dr. D. Gorla, Lic. M. Lamfri and Dr. S. Torrusio for the patience and guidance over the course of this work. Thanks are due to the two anonymous reviewers for valuable comments and advices for improving the text.

Appendix A. Supplementary data

Supplementary data to this article can be found online at https://doi.org/10.1016/j.ecoinf.2021.101351.

References

Albrieu-Llinás, G., Espinosa, M.O., Quaglia, A., Abril, M., Scavuzzo, C.M., 2018. Urban environmental clustering to assess the spatial dynamics of aedes aegypti breeding sites. Geospat. Health 13.

Andreo, V., Porcasi, X., Rodriguez, C., Lopez, L., Guzman, C., Scavuzzo, C.M., 2019. Time series clustering applied to eco-epidemiology: the case of aedes aegypti in córdoba, Argentina. In: 2019 XVIII workshop on information processing and control (RPIC). IEEE, pp. 93–98.

Aznar, V.R., Otero, M., Majo, M.S.D., Fischer, S., Solari, H.G., 2013. Modeling the complex hatching and development of aedes aegypti in temperate climates. Ecol. Model. 253, 44–55. https://doi.org/10.1016/j.ecolmodel.2012.12.004.

Bar-zeev, W., et al., 1957. The effect of density on the larvae of a mosquito and its influence on fecundity. Bull. Res. Counc. Isr. 220–228.

Briere, J.F., Pracros, P., Le Roux, A.Y., Pierre, J.s., 1999. A novel rate model of temperature-dependent development for arthropods. Environ. Entomol. 28, 22–29.

Burkart, R., Bárbaro, N.O., Sánchez, R.O., Gómez, D.A., 1999. Eco-regiones de la argentina.

Campos, R., Zanotti, G., Di Battista, C., Giménez, J., Fischer, S., 2020. Differential inhibition of egg hatching in aedes aegypti populations from localities with different winter conditions. Bull. Entomol. Res. First View 1–8. https://doi.org/10.1017/S0007485320000681.

Carrington, L.B., Seifert, S.N., Willits, N.H., Lambrechts, L., Scott, T.W., 2013. Large diurnal temperature fluctuations negatively influence aedes aegypti (diptera: Culicidae) life-history traits. J. Med. Entomol. 50, 43–51.

Chandrasegaran, K., Lahondère, C., Escobar, L.E., Vinauger, C., 2020. Linking mosquito ecology, traits, behavior, and disease transmission. Trends Parasitol. 36, 393–403. URL: http://www.ncbi.nlm.nih.gov/pubmed/32191853 https://doi.org/10.1016/j.pt.2020.02.001.

Chouakria, A.D., Nagabhushan, P.N., 2007. Adaptive dissimilarity index for measuring time series proximity. Adv. Data Anal. Class. 1, 5–21. https://doi.org/10.1007/s11634-006-0004-6.

Christophers, S.R., 1960. *Aedes aegypti*: The Yellow Fever Mosquito (CUP Archive).

Córdoba Epidemiological Report, 9 June 2020. Rec 2329.

Costa, E.A.P.D.A., Santos, E.M.D.M., Correia, J.C., Albuquerque, C.M.R.D., 2010. Impact of small variations in temperature and humidity on the reproductive activity and survival of aedes aegypti (diptera, culicidae). Rev. Brasil. Entomol. 54, 488–493.

Craig Jr., G.B., Vandehey, R.C., Hickey, W.A., 1961. Genetic variability in populations of aedes aegypti. Bull. World Health Organ. 24, 527.

De Majo, M., Zanotti, G., Campos, R., Fischer, S., 2019. Effects of constant and fluctuating low temperatures on the development of aedes aegypti (diptera: Culicidae) from a temperate region. J. Med. Entomol. 56 https://doi.org/10.1093/jme/tjz087.

Diaz-Nieto, L.M., Maciá, A., Perotti, M.A., Berón, C.M., 2013. Geographical limits of the southeastern distribution of aedes aegypti (diptera, culicidae) in Argentina. PLoS Negl. Trop. Dis. 7, e1963.

Ellis, A.M., Garcia, A.J., Focks, D.A., Morrison, A.C., Scott, T.W., 2011. Parameterization and sensitivity analysis of a complex simulation model for mosquito population dynamics, dengue transmission, and their control. Am. J. Trop. Med. Hygiene 85, 257–264.

Espinosa, M., Weinberg, D., Rotela, C.H., Polop, F., Abril, M., Scavuzzo, C.M., 2016. Temporal dynamics and spatial patterns of aedes aegypti breeding sites, in the context of a dengue control program in Tartagal (Salta province, Argentina). PLoS Negl. Trop. Dis. 10, e0004621.

de Estadística y Censos, I.N, 2010. Censo nacional de población, hogares y viviendas. URL. www.indec.gob.ar/ftp/cuadros/poblacion/censo2010_tomo1.pdf.

Focks, D.A., Haile, D.G., Daniels, E., Mount, G.A., 1993. Dynamic life table model for aedes aegypti (diptera: Culicidae): analysis of the literature and model development. J. Med. Entomol. 30, 1003–1017. https://doi.org/10.1093/jmedent/30.6.1003.

Francia, A., Maciá, A., 2011. Efectos de la competencia larval en los mosquitos de contenedores artificiales, aedes aegypti y culex pipiens (diptera: Culicidae) en condiciones semi-controladas. Rev. Soc. Entomol. Argentina 70, 305–315.

Goindin, D., Delannay, C., Ramdini, C., Gustave, J., Fouque, F., 2012. Parity and longevity of *Aedes aegypti* according to temperatures in controlled conditions and consequences on dengue transmission risks. PLoS One 10.

Gong, H., DeGaetano, A.T., Harrington, L.C., 2010. Climate-based models for west nile culex mosquito vectors in the northeastern US. Int. J. Biometeorol. 55, 435–446. https://doi.org/10.1007/s00484-010-0354-9.

Hone, J., Clutton-Brock, T.H., 2007. Climate, food, density and wildlife population growth rate. J. Anim. Ecol. 76, 361–367.

ISAGRO, 2021. Isagro. URL: http://webgis.isagro.org.ar/geoexplorer/composer/.

Jones, E., Oliphant, T., Peterson, P., et al., 2001. SciPy: Open source scientific tools for Python. URL: http://www.scipy.org/.

Kurtz, T., 1971. Limit theorems for sequences of jump markov processes. J. Appl. Probab. 8, 344–356.

Kurtz, T.G., 1970. Solutions of ordinary differential equations as limits of pure jump markov processes. J. Appl. Probab. 7, 49–58.

Lana, R.M., Carneiro, T.G., Honório, N.A., Codeço, C.T., 2014. Seasonal and nonseasonal dynamics of aedes aegypti in Rio de Janeiro, Brazil: fitting mathematical models to trap data. Acta Trop. 129, 25–32.

Lee, K.Y., Chung, N., Hwang, S., 2016. Application of an artificial neural network (ann) model for predicting mosquito abundances in urban areas. Ecol. Inform. 36, 172–180.

Legros, M., Otero, M., Aznar, V., Solari, H., Gould, F., Lloyd, A., 2016. Comparison of two detailed models of *Aedes aegypti* population dynamics. Ecosphere 7. https://doi.org/10.1002/ecs2.1515.

Liu-Helmersson, J., Brännström, Åke, Sewe, M.O., Semenza, J.C., Rocklöv, J., 2019. Estimating past, present, and future trends in the global distribution and abundance of the arbovirus vector aedes aegypti under climate change scenarios. Front. Public Health 7. https://doi.org/10.3389/fpubh.2019.00148.

Livdahl, T.P., Koenekoop, R.K., Futterweit, S.G., 1984. The complex hatching response of aedes eggs to larval density. Ecol. Entomol. 9, 437–442.

Logan, J., Wollkind, D., Hoyt, S., Tanigoshi, L., 1976. An analytic model for description of temperature dependent rate phenomena in arthropods. Environ. Entomol. 5, 1133–1140.

Marinho, R.A., Beserra, E.B., Bezerra-Gusmão, M.A., Porto, V.D.S., Olinda, R.A., dos Santos, C.A., 2016. Effects of temperature on the life cycle, expansion, and dispersion of aedes aegypti (diptera: Culicidae) in three cities in paraiba, Brazil. J. Vector Ecol. 41, 1–10.

Montes, M., Silvetti, L., Ferreyra, M., Molina, S.I., Florentina, D., Argañaraz, C.I., Horenstein, M.B., Gleiser, R.M., 2020. Seasonal variations of diptera assemblages in urban green patches of córdoba city, Argentina: same richness, different composition. Rev. Soc. Entomol. Argentina 79.

NASA, 2021. National Aeronautics and Space Administration. URL: https://www.nasa.gov/. accessed: 2020-06-15.

Nayar, J., Sauerman Jr., D., 1975. The effects of nutrition on survival and fecundity in Florida mosquitoes part 3. Utilization of blood and sugar for fecundity. J. Med. Entomol. 12, 220–225.

NOAA, 2021. National Oceanic and Atmospheric Administration. URL: https://www.noaa.gov/. accessed: 2020-06-15.

Organization, W.H, 2010. Dengue Guidelines for Diagnosis, Treatment, Prevention and Control. World Health Organization. URL: https://www.xarg.org/ref/a/9241547871/.

Organization, W.H, 2020. Dengue and Severe Dengue. URL. https://www.who.int/news-room/fact-sheets/detail/dengue-and-severe-dengue.

Otero, M., Solari, H.G., Schweigmann, N., 2006. A stochastic population dynamics model for aedes aegypti: formulation and application to a city with temperate climate. Bull. Math. Biol. 68, 1945–1974. https://doi.org/10.1007/s11538-006-9067-y.

Otero, M., Schweigmann, N., Solari, H.G., 2008. A stochastic spatial dynamical model for aedes aegypti. Bull. Math. Biol. 70, 1297.

Porcasi, X., Rotela, C.H., Introini, M.V., Frutos, N., Lanfri, S., Peralta, G., Elia, E.A.D., Lanfri, M.A., Scavuzzo, C.M., 2012. An operative dengue risk stratification system in Argentina based on geospatial technology. Geospat. Health 6, 31–42.

Porcasi, X., Andreo, V., Aguirre, E., Rojas, N., Rubio, J., Frutos, N., Guzman, C., Lopez, L., 2019. Spatial analysis of aedes aegypti activity for public health surveillance. In: 2019 XVIII Workshop on Information Processing and Control (RPIC). IEEE, pp. 214–217.

Powell, J.R., Tabachnick, W.J., 2013. History of domestication and spread of *Aedes aegypti* - a review. Mem. Inst. Oswaldo Cruz 108, 11–17. https://doi.org/10.1590/0074-0276130395.

Rojas, M.N.R., López, L., Guzmán, C., Scavuzzo, C.M., Porcasi, X., Lanfri, M., Aguirre, E., Ferreyra, M.F.G., Lighezzolo, A., Albornoz, C., 2017. Use of geospatial tools for decision-making in the arboviruses prevention and control, in the Cordoba city, Argentina. In: 2017 XVII Workshop on Information Processing and Control (RPIC). IEEE, pp. 1–5.

Romanenko, V.A., 1961. Computation of the autumn soil moisture using a universal relationship for a large area. Proc. Ukrain. Hydrometeorol. Res. Inst. 3, 12–25. URL: https://ci.nii.ac.jp/naid/10015209318/en/.

Romeo Aznar, V., Alem, I., De Majo, M.S., Byttebier, B., Solari, H.G., Fischer, S., 2018. Effects of scarcity and excess of larval food on life history traits of aedes aegypti (diptera: Culicidae). J. Vector Ecol. 43, 117–124.

Rotela, C., Lopez, L., Céspedes, M.F., Barbas, G., Lighezzolo, A., Porcasi, X., Lanfri, M.A., Scavuzzo, C.M., Gorla, D.E., 2017. Analytical report of the 2016 dengue outbreak in córdoba city, Argentina. Geospat. Health 12 (2), 226–236. https://doi.org/10.4081/gh.2017.564.

Rubio, A., Cardo, M.V., Vezzani, D., Carbajo, A.E., 2020a. Aedes Aegypti Spreading in South America: New Coldest and Southernmost Records, 115. Memórias do Instituto Oswaldo Cruz, e190496. URL: https://www.ncbi.nlm.nih.gov/pmc/articles/PMC7207151/ https://doi.org/10.1590/0074-02760190496.

Rubio, A., Cardo, M.V., Vezzani, D., Carbajo, A.E., 2020b. Aedes Aegypti Spreading in South America: New Coldest and Southernmost Records. Mem Inst Oswaldo Cruz, Rio de Janeiro 115, e190496.

de la Salud/Organización Mundial de la Salud, O.P, 20 June 2020. Actualización Epidemiológica Dengue y Otras Arbovirosis. OPS/OMS, Washington, D.C. URL: https://www.paho.org/es/file/66649/download?token=yqSF_9lr.

Scavuzzo, J.M., Trucco, F., Espinosa, M., Tauro, C.B., Abril, M., Scavuzzo, C.M., Frery, A. C., 2018. Modeling dengue vector population using remotely sensed data and machine learning. Acta Trop. 185, 167–175.

Schweigmann, N., Orellano, P., Kuruc, J., Vera, M., Vezzani, D., Méndez, A., 2002. Distribución y abundancia de aedes aegypti (diptera: Culicidae) en la ciudad de buenos aires. Actual. Artropodol. Sanit. Argentina 155–160.

Sharpe, P.J., DeMichele, D.W., 1977. Reaction kinetics of poikilotherm development. J. Theor. Biol. 64, 649–670. https://doi.org/10.1016/0022-5193(77)90265-x.

Sharpe, P.J., Curry, G.L., DeMichele, D.W., Cole, C.L., 1977. Distribution model of organism development times. J. Theor. Biol. 66, 21–38. URL: http://www.sciencedirect.com/science/article/pii/0022519377903095 https://doi.org/10.1016/0022-5193(77)90309-5.

Souza-Neto, J.A., Powell, J.R., Bonizzoni, M., 2019. *Aedes aegypti* vector competence studies: a review. Infect. Genet. Evol. 67, 191–209. https://doi.org/10.1016/j.meegid.2018.11.009.

Tran, A., LÁmbert, G., Lacour, G., Benoít, R., Demarchi, M., Cros, M., Cailly, P., Aubry-Kientz, M., Balenghien, T., Ezanno, P., 2013. A rainfall- and temperature-driven abundance model for aedes albopictus populations. Int. J. Environ. Res. Public Health 10, 1698–1719. https://doi.org/10.3390/ijerph10051698.

UCAR, 2021. University Corporation for Atmospheric Research. URL: https://www.ucar.edu/. accessed: 2020-08-06.

Valdez, L., Sibona, G., Diaz, L., Contigiani, M., Condat, C., 2017. Effects of rainfall on culex mosquito population dynamics. J. Theor. Biol. 421, 28–38. https://doi.org/10.1016/j.jtbi.2017.03.024.

Vezzani, D., Carbajo, A.E., 2008. Aedes aegypti, Aedes albopictus, and dengue in Argentina: current knowledge and future directions. Mem. Inst. Oswaldo Cruz 103, 66–74. https://doi.org/10.1590/S0074-02762008005000003.

Vezzani, D., Rubio, A., Velazquez, S., Schweigmann, N., Wiegand, T., 2005. Detailed assessment of microhabitat suitability for aedes aegypti (diptera: Culicidae) in Buenos Aires, Argentina. Acta Trop. 95, 123–131.

Wong, J., Stoddard, S.T., Astete, H., Morrison, A.C., Scott, T.W., 2011. Oviposition site selection by the dengue vector aedes aegypti and its implications for dengue control. PLoS Negl. Trop. Dis. 5, e1015.

Yang, G.J., Bradshaw, C.J., Whelan, P.I., Brook, B.W., 2008. Importance of endogenous feedback controlling the long-term abundance of tropical mosquito species. Popul. Ecol. 50, 293–305.

Yang, G.J., Brook, B.W., Bradshaw, C.J., 2009. Predicting the timing and magnitude of tropical mosquito population peaks for maximizing control efficiency. PLoS Negl. Trop. Dis. 3, e385.